ChemComm

COMMUNICATION

View Article Online
View Journal | View Issue

Cite this: *Chem. Commun.*, 2017, 53, 4465

Received 12th February 2017,
Accepted 24th March 2017

DOI: 10.1039/c7cc01122a

rsc.li/chemcomm

Dual-mode humidity detection using a lanthanide-based metal–organic framework: towards multifunctional humidity sensors†

Yuan Gao,[a] Pengtao Jing,[ab] Ning Yan,[a] Michiel Hilbers,[a] Hong Zhang,[ab] Gadi Rothenberg[a] and Stefania Tanase*[a]

Combined photoluminescence and impedance spectroscopy studies show that a europium-based metal–organic framework behaves as a highly effective and reliable humidity sensor, enabling dual-mode humidity detection.

Humidity sensors are used intensively in chemical processes, bio-engineering, and environmental science.[1,2] Their various applications include food processing and storage,[3,4] monitoring of oil pipelines,[5] and *in situ* monitoring in medical diagnosis.[6,7] Each application field requires different operating conditions, and so various types of humidity sensors exist. Generally, humidity sensors can be divided into three major groups: electronic, optical and accoustic.[8] Typical sensing materials are ceramics, semiconductors and polymers,[9–11] each of which has its own merits. However, different sensing materials also have different limitations. Sensors based on inorganic oxides require high temperatures and suffer from cross-sensitivity and baseline drift, while those based on organic polymers suffer from long response times and hysteresis.[12]

Electronic humidity sensing is the dominant technology today.[8] These sensors are relatively simple and inexpensive. Their main disadvantages include frequent calibration, low detection sensitivity, poor linearity and relatively long response times.[13] Optical sensing is emerging as an alternative technology thanks to the development of fibre-optic technologies.[14,15] Optical sensors are faster and more robust compared with the electronic ones, and they are more attractive for the chemical industry where flammable solvents are frequently used. Other advantages include the ease of fabrication and possibilities for both remote and *in situ* monitoring.[16,17] State-of-the-art optical humidity sensors use organic fluorescent molecules as sensing groups, but their reusability is problematic.[18,19] Current research is also exploring the use of acoustic waves to measure humidity.[8]

Metal–organic framework (MOF) materials are attractive candidates for humidity sensing.[20,21] Their advantage is the large surface-to-volume ratios available for interaction with analytes (*e.g.* water molecules).[22,23] This can increase their sensitivity and speed of response compared to conventional thin film sensing layers. Specifically, lanthanide-based MOFs (LnMOFs) are appealing candidates as optical sensing materials because of their narrow emission and high colour purity resulting from the lanthanide emitters.[24–28] The guest molecules in the host MOF influence the light absorption and emission profile of the lanthanide ions.[29] Several LnMOFs are reported as humidity sensing materials.[30,31] Recent studies also show that LnMOFs can have proton conducting properties.[32–34] However, as far as we know there is no example of such humidity sensing materials that combine both electronic detection and optical detection. Such versatile materials would open opportunities for designing new multi-purpose sensors.

Earlier, we showed that LnMOFs can be designed to give high proton conductivity.[35] Inspired by these results, we set out to apply this family of materials to humidity sensing. Here we report the humidity sensing behavior of two isostructural europium-based MOFs, $[Eu(H_2O)_2(mpca)_2Eu(H_2O)_6M(CN)_8]\cdot nH_2O$ (herein EuM, where mpca = 2-pyrazine-5-methyl-carboxylate, M = Mo, W), which have a robust 3D network with highly hydrophilic open channels filled with water molecules. We compare their performance using both electronic and optical detection responses and show that they have excellent sensitivity and reusability. To the best of our knowledge, this is the first report of a dual-mode humidity sensing molecular material.

Previous structural analysis[36,37] showed that the 3D structure of the EuM MOFs is comprised of two-dimensional networks of alternating diamond-like $Eu_2M_2(CN)_4$ rings and octagonal $Eu_4M_4(CN)_8$ rings, which are connected by $[Eu(H_2O)_6]^{3+}$ ions (abbreviated as Eu1) *via* the carboxylate group of $mpca^-$ ligands from adjacent sheets (Fig. S1, ESI†). These Eu^{3+} ions

[a] *Van't Hoff Institute for Molecular Sciences, University of Amsterdam, Science Park 904, 1098 XH Amsterdam, The Netherlands. E-mail: s.grecea@uva.nl, h.zhang@uva.nl*

[b] *State Key Laboratory of Luminescence and Applications, Changchun Institute of Optics, Fine Mechanics and Physics, Chinese Academy of Sciences, Changchun 130033, P. R. China*

† Electronic supplementary information (ESI) available: Experimental details, IR, PXRD, TGA and photoluminescence spectra. See DOI: 10.1039/c7cc01122a

are eight-coordinated. Conversely, the Eu^{3+} ions in the 2D network (abbreviated as Eu2) are nine-coordinated due to the *N*,*O*-bidentate binding of two anionic $mpca^{-}$ ligands, three cyanide ions, one water molecule and one methanol molecule (Fig. S1, ESI†). By exposing the MOFs to ambient conditions, the coordinated methanol is replaced by a water molecule.[37]

The solid-state excitation and emission spectra of the EuM materials were recorded under ambient conditions (Fig. S2, ESI†). Upon excitation at 280 nm, five main peaks of Eu^{3+} are observed at $^5D_0 \rightarrow {}^7F_0$ (582 nm), $^5D_0 \rightarrow {}^7F_1$ (596 nm), $^5D_0 \rightarrow {}^7F_2$ (617 nm), $^5D_0 \rightarrow {}^7F_3$ (655 nm), and $^5D_0 \rightarrow {}^7F_4$ (705 nm). The $^5D_0 \rightarrow {}^7F_2$ transition is more pronounced than the $^5D_0 \rightarrow {}^7F_1$ transition, indicating that the coordination environment of the Eu^{3+} ions is asymmetric,[38] in agreement with the crystal structure analysis.[37] When monitoring the characteristic 617 nm emission for Eu^{3+}, the excitation spectrum shows a broad excitation band between 250 and 350 nm with a maximum value at 290 nm. We assign this band to the $\pi \rightarrow \pi^*$ electron transition of the ligand, as the EuM MOFs have similar absorption bands (Fig. S3, ESI†).

For the as-synthesized EuM MOFs, the $^5D_0 \rightarrow {}^2F_7$ decay curves monitored at 617 nm could be explained by a bi-exponential behaviour (Fig. S4, ESI†). Two decay constants, denoted as τ_1 (Eu1) and τ_2 (Eu2), are obtained. This is in agreement with the existence of two different crystallographic Eu^{3+} centers. Eu1, which has six coordinated water molecules, has a shorter lifetime than Eu2 with only two coordinated water molecules. This demonstrates that the coordinated water serves as efficient oscillators for the Eu^{3+} emission properties. Even though the two compounds are isostructural, the EuW MOF showed longer lifetime (6.7, 58.0 μs) than the EuMo MOF (6.3, 45.6 μs) (Fig. S4, ESI†). In view of these results we focused on the EuW material, monitoring the emission dynamics at every 60 s.

Fig. 1 shows that the emission decay of the EuW MOF increased with longer irradiation time, until the decay curves converged within 60 min. There are three important periods. The first corresponds to the first 20 min in which both τ_1 = 6.67 to 18.2 μs (Eu1) and τ_2 = 58.0 to 83.2 μs (Eu2) increased. Then, there is no obvious decay change between 20 and 60 min. This induction period suggests that the removal of the lattice water molecules leads to a stable framework, in agreement with our earlier studies.[32] After 60 min only one lifetime is detected.

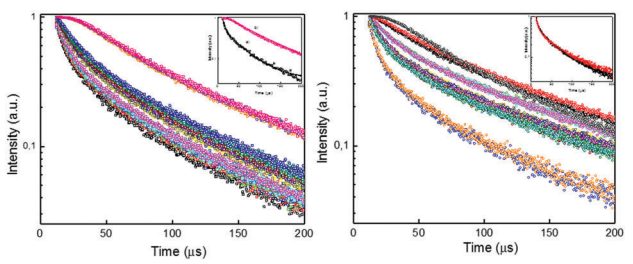

Fig. 1 Luminescence decay curves of the $^5D_0 \rightarrow {}^7F_2$ transition (λ_{em} = 617 nm) in the EuW MOF measured at every 60 s for as-synthesised material (right) and after water addition (left). The inset shows the fit to $f(x) = A_1 \exp(x/\tau_1) + A_2 \exp(x/\tau_2)$ at the start (a) and at the end (b) for the as-synthesised material (left) and as-synthesised and the rehydrated EuW MOF (right).

At the beginning of 61 min, however, when the removal of coordinated water occurs, the decay time increased sharply from 120 μs to 170 μs within 2 min, and then remains stable for 5 min (Fig. 1, left). This behavior suggests that some weak coordinated water molecules were removed giving a new stable framework. To confirm this hypothesis, we can estimate the number of Eu-bound water molecules using the previously[39,40] reported formula:

$$n = 1.05 \times \tau_{H_2O}^{-1} - 0.70 \ (\tau \text{ in ms})$$

Earlier studies[39,40] show that the OH oscillators act independently. This means that the rate of de-excitation *via* the weak vibronic coupling of the Ln^{3+} ion excited states with the OH oscillators of the coordinated water molecules is directly proportional to the number of OH oscillators in the first coordination sphere. To a reasonably good approximation the energy transfer to higher OH vibrational overtones is independent of the remaining ligands completing the coordination sphere of the Ln^{3+} ion.[39] This simple estimate shows that there are 8.05 Eu-bound water molecules at 61 min (τ = 120 μs) and only 5.01 Eu-bound water molecules at 63 min (τ = 170 μs). The results are again in excellent agreement with the previous studies,[38] demonstrating that the partial removal of the coordinated water leads to a highly stable framework. Note however that the above estimation cannot be used to calculate the Eu-bound water in the fully hydrated MOF material due to the complex de-excitation pathways. The coordinated water molecules participate in a reachable hydrogen bonding network with the oxygen atoms of the coordinated carboxylate ligands and of the lattice water molecules, as well as with nitrogen atoms from the neighboring terminal cyanide groups.

To prove that the above process is reversible, we ran control experiments adding water to the laser-irradiated sample (Fig. 1, right). The dropwise addition of 0.1 ml water resulted in a quick decrease of the signal lifetime from 170 μs in the dehydrated sample to 6.4 μs and 64.3 μs in the rehydrated material. These lifetimes fit with those observed for the as-synthesized material (6.7 μs, 57.6 μs), confirming the reversibility of dehydration–rehydration processes. The EuW MOF can trap the guest water molecules within 60 s, giving a quick and effective optical humidity sensing response. The EuMo MOF sample showed similar lifetime decay changes during the dehydration process (Fig. S5, ESI†), but these were less dramatic compared to those of the EuW MOF.

The above results show that our EuW MOF can sense relative humidity (RH) under 8.0% (calculated based on the water uptake), where most reported sensing materials cannot.[38] To demonstrate further the optical humidity sensing properties of this MOF (upon removal of the lattice water molecules), we studied its photoluminescence properties under different RH conditions. Most reported MOFs can detect humidity in the range between 5 and 85%.[31,41] Fig. 2 shows indeed that the emission properties are largely dependent on the RH, ranging from 0% to 100%, with a response time of 5 min in all cases, much shorter than the response time reported for LnMOFs (Table S1, ESI†). The inset

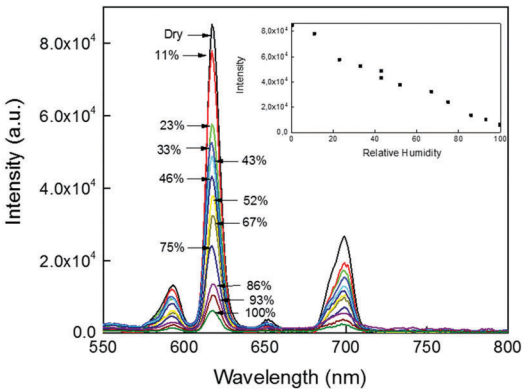

Fig. 2 Solid-state emission spectra of the EuW MOF activated at 80 °C and then exposed to various relative humidities (λ_{ex} = 280 nm). The inset is the linearization according to the humidity changes.

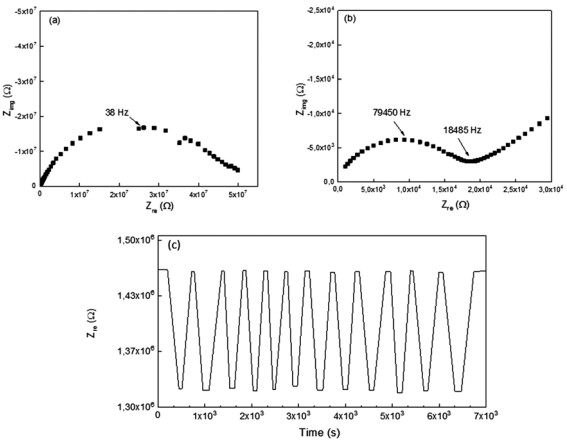

Fig. 3 Nyquist plots of the EuW MOF activated at 80 °C and measured at 21 °C under dry conditions (a) and 100% RH (b). Impedance response and recovery time of the EuW MOF measured at 21 °C and relative humidity (RH) variation between 53% and 100% (c).

in Fig. 2 shows the decreasing trend of emission intensity with increasing humidity, and a good linearity over broad humidity ranges. Thus, the EuW MOF can sense guest water molecules and is an effective material for optical humidity sensors. Notably, the FTIR spectrum and the PXRD pattern (Fig. S6 and S7, ESI†) of the as-synthesised and rehydrated samples are identical, demonstrating that this material retains its structural integrity during dehydration/hydration cycles, a key requirement for practical applications. Note that this luminescence-based sensing material has large detection ranges. If the environmental condition of the activated sample was considered as 0% RH, the sensing range is from 0% to 100% RH.

When used as a dielectric in a capacitor, a MOF material will change its permittivity depending on the amount of physisorbed water (guest water molecules). This is in fact the working principle of a capacitive humidity sensor. Therefore, we ran an EIS analysis using a sample at varied degrees of relative humidity (Fig. S8, ESI†), which shows the changes under different conditions. Fig. 3(a) shows the proton conductivities of EuW MOFs in the form of the Nyquist plots under dry conditions (10^{-10} S cm^{-1}). The value is 3 orders of magnitude higher at 100% RH. It also shows that the Nyquist plot for dry conditions is an inclined semicircle, while a clear upturned line along with the semicircle is observed at 100% RH (Fig. 3(b)). To understand the sensing mechanism and the temperature influence, we compared the impedance values at different temperatures, while keeping the relative humidity constant at 100%. The magnitude orders of the conductivity increase slightly from 10^{-5} to 10^{-4}. From these measurements we derived an Arrhenius activation energy of 0.37 eV, which is within the range of a Grotthuss transfer mechanism (Fig. S9, ESI†). Thus, an effective proton conduction path is achieved upon uptake of the guest water molecules. The resistance of EuW MOFs experiences a significant change of 10^3 magnitude difference. This confirms our previous studies on isostructural compounds that demonstrate the effective role of lattice water molecules in achieving high proton conductivities.[32]

The reversibility and reproducibility of the EuW sensing material were also examined through exposure/recovery cycles from low to high RH, and back. The sensor exhibits the highest sensitivity at 500 Hz. Thus, 500 Hz was selected as the testing frequency in subsequent experiments. Fig. 3, right, shows the response–recovery properties of EuW MOFs between 100% and 53% RH for five cycles measured. The peak (~1.30 MΩ) and trough (~1.48 MΩ) values changed slightly, showing good repeatability of the sensor. Importantly, this material does not show baseline drift, thus overcoming the hysteresis problem of many commercial sensors. These results confirm that the interactions between water and the surface of the MOF were dominated by physisorption.

The response time is defined as the time taken by a sensor to achieve 90% total impedance change. For the EuW MOF, the average response and recovery times are about 380 s (from 100% RH to 53% RH) and 390 s (from 53% RH to 100% RH). This recovery time is similar to the photoluminescence measurement (400 s), indicating strongly that the results reported here are highly reliable for sensing application.

In conclusion, we showed that a highly robust EuW MOF is an effective and highly reliable humidity sensor, using both electrical and optical detection methods. We foresee more research in the field of lanthanide-based MOFs as dual-mode humidity sensing materials. Such materials give opportunities for dual and multimode sensing that can be used in bio-sensing systems and to expand the dynamic sensing range. Dual signals resulting from the guest molecules and the nodes of the framework would enable recognition and quantification at the same time.

YG thanks the China Scholarship Council for a PhD fellowship. PJ acknowledges the Holland Research School of Molecular Chemistry for his research fellowship. This work is part of the Research Priority Area Sustainable Chemistry of the University of Amsterdam, http://suschem.uva.nl.

Notes and references

1 Z. Chen and C. Lu, *Sens. Lett.*, 2005, **3**, 274.
2 H. Farahani, R. Wagiran and M. N. Hamidon, *Sensors*, 2014, **14**, 7881.
3 L. Alwis, T. Sun and K. T. V. Grattan, *Measurement*, 2013, **46**, 4052.

4 S. L. Norman, A. Luechinger, E. K. Athanassiou, R. N. Grass and W. J. Stark, *Langmuir*, 2007, **23**, 3473.
5 M. Zubair and T. B. Tang, *Sensors*, 2014, **14**, 11351.
6 N. Yamazoe, *Sens. Actuators*, 1986, **10**, 379.
7 A. Tételin, C. Pellet, C. Laville and G. N'Kaoua, *Sens. Actuators, B*, 2003, **91**, 211–218.
8 W. H. Zhu, Z. M. Wang and S. Gao, *Inorg. Chem.*, 2007, **4**, 1337.
9 A. I. Buvailo, Y. Xing, J. Hines, N. Dollahon and E. Borguet, *ACS Appl. Mater. Interfaces*, 2011, **3**, 528.
10 S.-I. Ohira, P. K. Dasgupta and K. A. Schug, *Anal. Chem.*, 2009, **81**, 4183.
11 S. Neumeier, T. Echterhof, R. Bolling, H. Pfeifer and U. Simon, *Sens. Actuators, B*, 2008, **134**, 171.
12 S. Achmann, G. Hagen, J. Kita, I. M. Malkowsky, C. Kiener and R. Moos, *Sensors*, 2009, **9**, 1574.
13 A. L. Tiano, C. Koenigsmann, A. C. Santulli and S. S. Wong, *Chem. Commun.*, 2010, **46**, 8093.
14 J. E. Stumpel, D. J. Broer and A. P. Schenning, *Chem. Commun.*, 2014, **50**, 15839.
15 C. Liu, C. Yao, Y. Zhu, J. Ren and L. Ge, *Sens. Actuators, B*, 2015, **220**, 227.
16 W. E. Lee, Y. J. Jin, L. S. Park and G. Kwak, *Adv. Mater.*, 2012, **24**, 5604.
17 N. Suzuki, A. Fukazawa, K. Nagura, S. Saito, H. Kitoh-Nishioka, D. Yokogawa, S. Irle and S. Yamaguchi, *Angew. Chem., Int. Ed.*, 2014, **53**, 8231.
18 Y. Yu, X. M. Zhang, J. P. Ma, Q. K. Liu, P. Wang and Y. B. Dong, *Chem. Commun.*, 2014, **50**, 1444.
19 V. M. H. Mishra, M. S. Mehata, T. C. Pant and H. B. Tripathi, *J. Phys. Chem. A*, 2004, **108**, 2346.
20 D. J. Wales, J. Grand, V. P. Ting, R. D. Burke, K. J. Edler, C. R. Bowen, S. Mintova and A. D. Burrows, *Chem. Soc. Rev.*, 2015, **44**, 4290.
21 J. Heine and K. Müller-Buschbaum, *Chem. Soc. Rev.*, 2013, **42**, 9232.
22 Y. Y. Fu, C. X. Yang and X. P. Yan, *Chem. Commun.*, 2013, **49**, 7162.
23 D. Banerjee, Z. Hu and J. Li, *Dalton Trans.*, 2014, **43**, 10668.
24 D. Wang, J. Zhang, Q. Lin, L. Fu, H. Zhang and B. Yang, *J. Mater. Chem.*, 2003, **13**, 2279.
25 Z. Hu, B. J. Deibert and J. Li, *Chem. Soc. Rev.*, 2014, **43**, 58150.
26 S. Roy, A. Chakraborty and T. K. Maji, *Coord. Chem. Rev.*, 2014, **273**, 139.
27 K. Müller-Buschbaum, F. Beuerle and C. Feldmann, *Microporous Mesoporous Mater.*, 2015, **216**, 171.
28 S.-N. Zhao, L.-J. Li, X.-Z. Song, M. Zhu, Z.-M. Hao, X. Meng, L.-L. Wu, J. Feng, S.-Y. Song, C. Wang and H.-J. Zhang, *Adv. Funct. Mater.*, 2015, **25**, 1463.
29 J. Rocha, L. D. Carlos, F. A. Paz and D. Ananias, *Chem. Soc. Rev.*, 2011, **40**, 926.
30 D. Wu, X. Guo, H. Sun and A. Navrotsky, *J. Phys. Chem.*, 2016, **120**, 7562.
31 Y. Yu, J.-P. Ma and Y.-B. Dong, *CrystEngComm*, 2012, **14**, 7157.
32 R. M. P. Colodrero, K. E. Papathanasiou, N. Stavgianoudaki, P. Olivera-Pastor, E. R. Losilla, M. A. G. Aranda, L. León-Reina, J. Sanz, I. Sobrados, D. Choquesillo-Lazarte, J. M. García-Ruiz, P. Atienzar, F. Rey, K. D. Demadis and A. Cabeza, *Chem. Mater.*, 2012, **24**, 3780.
33 J. M. Taylor, K. W. Dawson and G. K. Shimizu, *J. Am. Chem. Soc.*, 2013, **135**, 1193.
34 M. Zhu, Z. M. Hao, X. Z. Song, X. Meng, S. N. Zhao, S. Y. Song and H. J. Zhang, *Chem. Commun.*, 2014, **50**, 1912–1914.
35 Y. Gao, R. Broersen, W. Hageman, N. Yan, M. C. Mittelmeijer-Hazeleger, G. Rothenberg and S. Tanase, *J. Mater. Chem. A*, 2015, **3**, 22347.
36 S. Tanase, L. J. de Jongh, F. Prins and M. Evangelisti, *ChemPhysChem*, 2008, **9**, 1975.
37 S. Tanase, M. C. Mittelmeijer-Hazeleger, G. Rothenberg, C. Mathonière, V. Jubera, J. M. M. Smits and R. de Gelder, *J. Mater. Chem.*, 2011, **21**, 15544.
38 K. Andrew F, D. Foster and F. S. Richardson, *Chem. Phys. Lett.*, 1983, **95**, 507.
39 W. D. Horrocks and D. R. Sudnick, *J. Am. Chem. Soc.*, 1979, **101**, 334.
40 G. R. Choppin and D. R. Peterman, *Coord. Chem. Rev.*, 1998, **174**, 283.
41 X. Liang, F. Zhang, H. Zhao, W. Ye, L. Long and G. Zhu, *Chem. Commun.*, 2014, **50**, 6513.

